

Article

Nickel Stabilized Si/Ni/Si/Ni Multi-Layer Thin-Film Anode for Long-Cycling-Life Lithium-Ion Battery

Yonhua Tzeng *, Yu-Yang Chiou and Aurelius Ansel Wilendra

Institute of Microelectronics, National Cheng Kung University, Tainan 70101, Taiwan;
q16121135@gs.ncku.edu.tw (Y.-Y.C.); q16125016@gs.ncku.edu.tw (A.A.W.)

* Correspondence: tzengyo@mail.ncku.edu.tw

Abstract: Silicon-based anodes suffer from the loss of physical integrity due to large volume changes during alloying and de-alloying processes with electrolytes. By integrating electrochemically inert, physically strong, ductile nickel layers with a multi-layered thin-film silicon anode, the long-life cycling of the Si/Ni/Si/Ni anode was demonstrated. A capacity retention of 82% after 200 cycles was measured, surpassing the performance of conventional silicon thin-film anodes. This is attributed to the effective suppression of internal local stress induced by nonuniform volume expansion by the nickel layers. These findings offer a promising pathway towards the practical implementation of high-capacity silicon-based anodes in advanced lithium-ion batteries.

Keywords: lithium-ion battery; silicon; multi-layer thin film; anode; nickel; large surface area; protective layer

1. Introduction

Commercial lithium-ion batteries currently rely on graphite-based anodes. However, the surging demand for high-capacity energy storage solutions, particularly in electrical vehicles [1] and other applications, necessitates a departure from conventional graphite anodes, which exhibit a limited specific capacity of 372 mAh/g. Silicon-based anodes, with their exceptional specific capacity of 3579 (Li₁₅Si₄)–4200 (Li₂₂Si₅) mAh/g and relatively low discharge potential (approximately 0.4 V vs. Li/Li⁺), emerge as a compelling alternative to address this capacity limitation.

Despite their promising characteristics, silicon anodes confront several critical challenges that hinder their practical implementation. The inherent low electrical conductivity of silicon and its substantial volume expansion (approximately 400%) during charge-discharge cycles are particularly problematic. These factors lead to increased internal resistance and stress [2], reduced Coulombic efficiency, and ultimately, degraded long-term performance during cycling [3].

To address these challenges, researchers have explored various strategies. Structurally, the use of silicon nanoparticles [4,5], nanotubes [6,7], nanowires [8,9], and thin films [10,11] have been investigated. Additionally, surface modification techniques, such as carbon (C) coating [12] and carbon composites [13], diamond nanoparticles (ND) [14], copper (Cu) [15], and other materials [16,17], have been employed to mitigate the potential damage caused by the volumetric expansion of silicon.

Multi-layer thin-film structures, such as Si-Y multi-layer thin films, as anode materials of high-capacity lithium-ion batteries [18] deliver a high reversible capacity of 2450 mAh/g under a current density of 0.4 C after 50 cycles. The volumetric expansion of silicon can be



Academic Editor: Marco Giorgetti

Received: 9 December 2024

Revised: 20 January 2025

Accepted: 22 January 2025

Published: 25 January 2025

Citation: Tzeng, Y.; Chiou, Y.-Y.; Wilendra, A.A. Nickel Stabilized Si/Ni/Si/Ni Multi-Layer Thin-Film Anode for Long-Cycling-Life Lithium-Ion Battery. *Batteries* **2025**, *11*, 46. <https://doi.org/10.3390/batteries11020046>

Copyright: © 2025 by the authors. Licensee MDPI, Basel, Switzerland. This article is an open access article distributed under the terms and conditions of the Creative Commons Attribution (CC BY) license (<https://creativecommons.org/licenses/by/4.0/>).

effectively suppressed by forming a Fe layer between Si layers, which was tested using the constant charge and discharge current of $30 \mu\text{A}/\text{cm}^2$ between 0 and 1.2 V at 30°C [19].

Yang et al. [20] reported a multi-layer thin-film structure consisting of carbon/silicon/carbon/silicon (with the outer carbon layer in contact with the electrolyte), fabricated through magnetron sputtering. The protective carbon layers significantly enhance the cycling stability of the silicon anode. The initial discharge specific capacity was approximately 2045.9 mAh/g, which stabilized at around 1500 mAh/g after 200 cycles, resulting in a capacity retention rate of 85.4%. Salah et al. [21] reported silicon/tin thin-film anodes for low- and high-power-density lithium-ion batteries.

Tzeng et al. [14] reported a multi-layer thin-film silicon-based anode with nanoscale diamond particles as an interfacial layer and the surface layer. Diamond particles decorated with silicon thin films result in better uniform lithium-ion flux and an improved wettability of the anode to the electrolyte. Both effects enhanced the physical integrity of the silicon thin-film anode and the cycling performance.

FU et al. [22] reported a multi-layer electrode made of NiO/SnO₂ by alternating magnetron sputtering. Ni nanoparticles (NP) formed from NiO can lower the Li-O bonding energy, thereby enhancing the transition reaction from Sn/Li₂O to SnO₂, further decreasing the Li loss. Additionally, Ni can also enhance the conductivity and alleviate volume expansion. The NiO/SnO₂ multi-layer electrode exhibits a high ICE of 92.3% and retains ~97% capacity at a low test current density. As shown in Table S1, silicon offers a much higher specific capacity and a lower potential versus Li/Li⁺ than tin, making it an attractive anode material. However, the substantial volume expansion (300–400%) of silicon during cycling compared to tin (260%) results in internal stress, which may cause structural degradation and capacity loss. Furthermore, in their study, the maximum current density utilized in the C-rate tests was limited to a low current density of 5 A/g. Due to the use of oxide materials, the resistance values obtained from EIS measurements were high and cycling performance at a high test current density left much room for improvement.

In this study, nickel was used as an interfacial layer and a surface layer in a nickel/silicon multi-layer thin-film anode. We employed thermal evaporation to deposit approximately 100 nm of silicon onto a copper foil substrate, followed by the deposition of a 20 nm nickel (Ni) layer directly onto the silicon surface. This process was repeated twice to yield a multi-layer Si/Ni/Si/Ni anode structure. The Ni layer plays a pivotal role in this anode. As the surface layer, it prevents potential side reactions by blocking direct contact between the electrolyte and the silicon. Additionally, it provides mechanical strength to accommodate the volume changes of silicon during cycling. This protective function safeguards the overall structure from damage caused by the silicon's expansion, thereby significantly improving the long-term cycling performance of the battery.

2. Materials and Methods

2.1. Electrode Preparation

All electrodes were fabricated through thermal evaporation to deposit thin films. N-type crystalline silicon (99.999% purity) and a Ni slug (99.995% purity) served as the evaporation sources, while copper foils (14 mm in diameter) were used as current collectors.

The deposition process was conducted under a background pressure of approximately 5×10^{-6} torr, with a substrate temperature set at 250°C . The deposition rate was controlled between 0.5 and 1 nm/s.

Prior to silicon deposition, the Cu foil was thoroughly cleaned in an ultrasonic bath using acetone, ethanol, and deionized water to remove surface contaminants. Following this cleaning step, thin-film deposition was initiated. For the reference silicon anode, a single 200 nm layer of silicon was directly deposited onto the Cu foil surface. In contrast,

the Si/Ni anode was fabricated by sequentially depositing a 100 nm silicon layer and a 20 nm nickel layer. This sequence was repeated twice to form the Si/Ni/Si/Ni multi-layer anode structure (Figure 1).

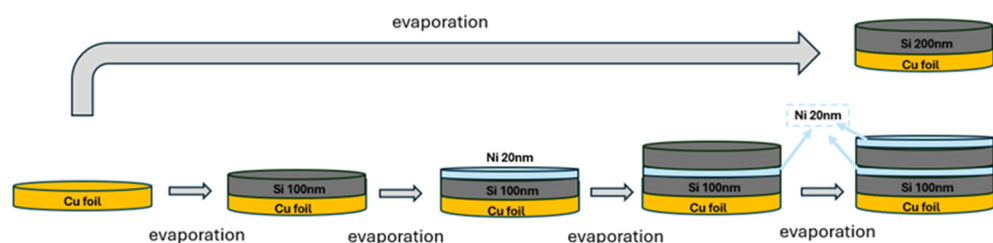


Figure 1. Schematic diagram of the fabrication processes for a Si-based anode and a Si/Ni/Si/Ni thin-film anode.

2.2. Fabrication of Coin Cells

The thin-film electrodes were assembled into CR2032 coin cells paired with lithium metal cathodes within an argon-filled glove box. Rigorous control was maintained to ensure oxygen and moisture levels remained below 0.3 ppm.

The electrolyte comprised a 1 M LiPF₆ solution dissolved in a 2:1:2 volume ratio of dimethyl carbonate (DMC), diethyl carbonate (DEC), and ethylene carbonate (EC). Additionally, 10 wt.% of fluoroethylene carbonate (FEC) was incorporated into the electrolyte composition.

2.3. Electrochemical Testing

Galvanostatic discharge/charge tests were performed using a BAT battery testing system within a voltage range of 0.01–1.5 V for the half-cells under the test current density of 0.05 mA/cm². For the C-rate stepped tests, the current density was gradually increased from 0.05 mA/cm² to 1.5 mA/cm² and then reduced back to 0.05 mA/cm² to evaluate electrode stability under varied current conditions. Electrochemical impedance spectroscopy (EIS) and cyclic voltammetry (CV) analyses were conducted using an Autolab instrument (Metrohm AUTOLAB BV, Taipei, Taiwan). EIS measurements were performed over a frequency range from 0.1 Hz to 100 kHz, while CV scans were conducted at room temperature with a scan rate of 0.05 mV/s.

2.4. Electrode Characterization

To analyze the electrode surface morphology before and after cycling, the coin cells were disassembled within an argon-filled glove box, and the electrodes were retrieved. The retrieved electrodes were rinsed with diethyl carbonate (DEC) to remove residual electrolyte and air-dried within the glove box. Scanning electron microscopy (SEM, Hitachi-SU8000, Taipei, Taiwan) was employed to examine the surface morphology of the electrode.

3. Results

Figure 2a,b present the XRD analysis showing that the elevated temperature during deposition caused alloying reactions between Cu and Si, as well as between Si and Ni, leading to the formation of alloy layers. Figure 2b shows a magnified XRD spectrum of Figure 2a to display the weaker signals. These alloy layers significantly improved interfacial contact between layers, functioning as an “alloy binder” to enhance the overall bonding strength of the materials. The lack of a distinct Si signal in the XRD pattern is likely due to the amorphous nature of the silicon.

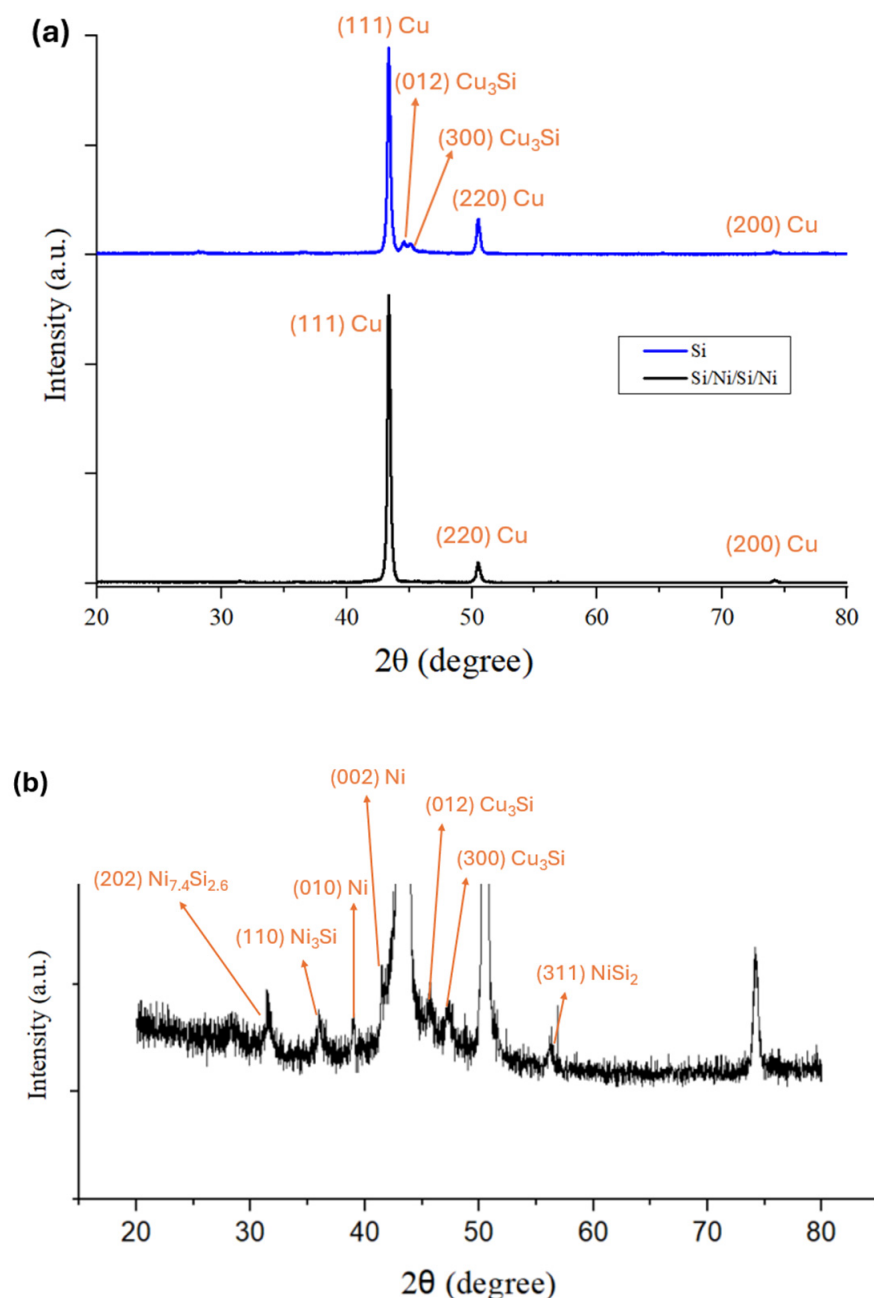


Figure 2. XRD analysis of (a) a Si anode and a Si/Ni/Si/Ni thin-film anode; (b) magnified intensity of a Si/Ni/Si/Ni thin-film anode.

Figure 3a,b present scanning electron microscopy (SEM) images of a silicon thin-film anode and a Si/Ni/Si/Ni multi-layer thin-film anode, respectively. The Si thin-film anode (Figure 3a) exhibits a nonuniform surface morphology. The Ni top layer (Figure 3b) formed relatively uniform semispherical structures and numerous pores in between and, thus, facilitated more uniform lithium-ion transport. Because nickel and its compound are more ductile than silicon, the surface passivation layer may enhance the physical integrity of the anode. This enhanced surface area with special structures improves the contact area between the electrolyte and the anode [23], facilitating efficient lithium-ion transport under a high current density [24]. Additionally, a uniform and rough surface enhances the adhesion between the solid electrolyte interphase (SEI) and the anode, reducing interfacial resistance to charge transport and contributing to an improved overall performance.

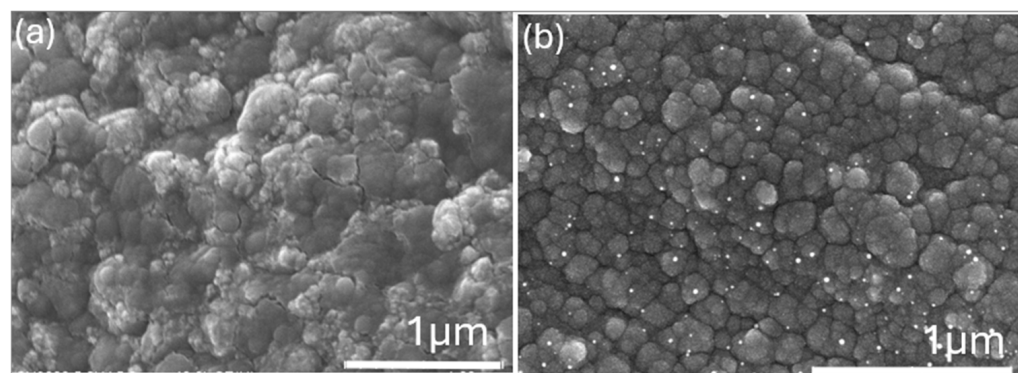


Figure 3. SEM images of the top view of (a) a Si thin-film anode and (b) a Si/Ni/Si/Ni thin-film anode.

Figure 4a,b show the cyclic voltammetry (CV) profiles of the electrodes, where the cathodic and anodic peaks correspond to lithium-ion insertion and extraction processes, respectively. The high degree of overlap in the Si/Ni/Si/Ni thin-film anode's CV curves after the first cycle indicates the excellent cycling stability and high reversible capacity of this anode. The oxidation peaks observed at approximately 0.3 V and 0.51 V (detailed values are provided in Table S2) during the de-alloying process are attributed to the phase transition from Li_xSi_y to amorphous silicon. The delithiation process of Li_xSi_y is typically a multi-step process. Peak A at 0.3V might correspond to the gradual transition from high-lithium-content alloys (such as $\text{Li}_{15}\text{Si}_4$ and $\text{Li}_{22}\text{Si}_5$) to lower-lithium-content phases (such as $\text{Li}_{13}\text{Si}_4$ and Li_7Si_3). At peak B at 0.51V, the structure gradually transformed into a low-lithium-content silicon phase ($\text{Li}_{3.75}\text{Si}$) or amorphous silicon.

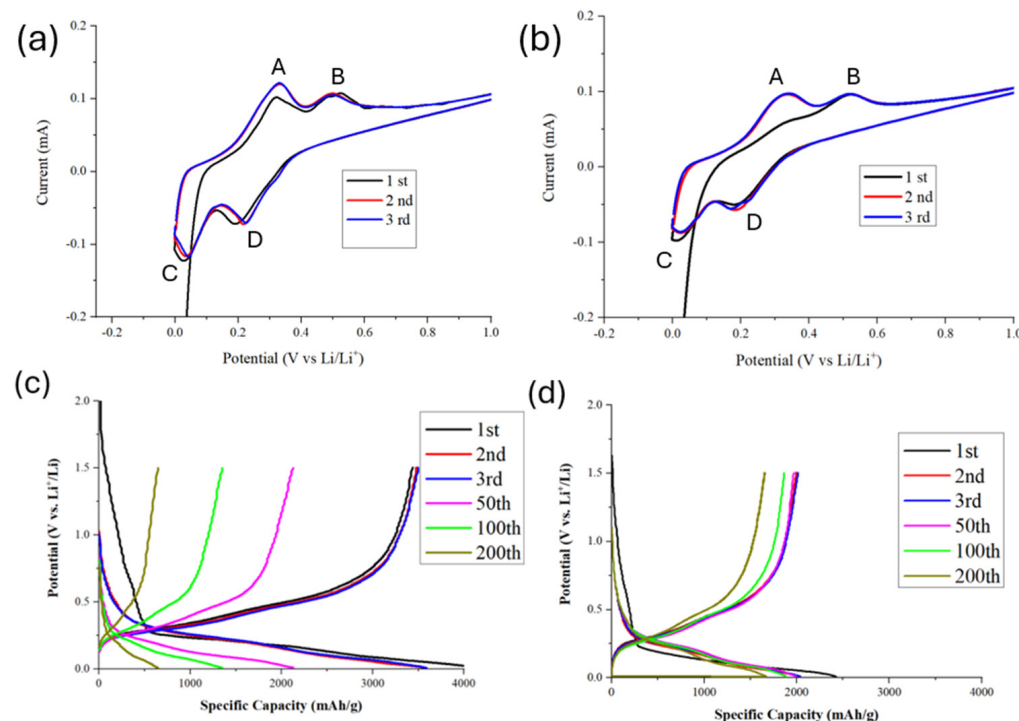


Figure 4. CV curve of (a) a Si thin-film anode and (b) a Si/Ni/Si/Ni thin-film anode; charge–discharge curves of different cycling numbers for the (c) Si thin-film anode and (d) the Si/Ni/Si/Ni thin-film anode.

During alloying, lithium ions were inserted into amorphous silicon, resulting in the formation of different amorphous Li_xSi_y phases at around 0.03 V and 0.19 V, as indicated

by the two reduction peaks. At peak D of 0.19 V, $\text{Li}_{12}\text{Si}_7$ was formed. Higher Li phases (such as $\text{Li}_{15}\text{Si}_4$, $\text{Li}_{21}\text{Si}_5$) were formed at peak C at approximately 0.02V [25].



As shown in Figure 4c,d, the first cycle charge capacity of the Si thin-film anode (3438 mAh/g) was nearly 1.5 times that of the Si/Ni/Si/Ni thin-film anode (1992 mAh/g) (Figure 4d). The reduced capacity in the Si/Ni/Si/Ni anode can be attributed to the presence of Ni layers, which have a higher density (8.9 g/cm^3) than Si (2.33 g/cm^3). The increased mass loading of Ni reduced the overall specific capacity.

The Ni interfacial layer and the surface layer play significant roles in stabilizing the thin-film Si anode. Zhang et al. reported that a silicon anode having been subjected to prolonged exposure to high potentials led to the formation of a soft and thick SEI layer and made it more prone to cracking after multiple cycles of charging and discharge [26]. Figure 4c,d, show that a slow decline of the first-cycle lithiation curve for a thin-film Si anode is correlated with the substantial growth of a thick SEI layer on the Si thin-film anode. SEI formed by reactions of Si with the electrolyte is mostly irreversible. This gradual voltage drop during the initial lithiation stage is attributed to the significant lithium-ion consumption, which is required for the substantial SEI formation and buildups. This slow decline is in clear contrast with the fast decline of the first-cycle lithiation curve for a Si/Ni/Si/Ni anode, which exhibits a much thinner SEI.

Joshi et al. showed that transition metals accelerate the growth of inorganic components within the SEI layer [27]. Inorganic phases exhibit high elastic moduli [28], and contribute to a more mechanically robust SEI layer, which suppresses crack formation and reduces the exposure of new silicon surfaces. Excessive growth of the SEI on fresh silicon surfaces is, thus, minimized. Moreover, the intermetallic compound formed by Ni with Si acts as a binder to prevent silicon from cracking and an electrochemically inactive passivation layer for protecting silicon from reactions with the electrolyte. This inactive interlayer does not participate in electrochemical reactions with the electrolyte and remains dimensionally stable during repeated electrochemical cycling [29], further improving the physical integrity of the Si/Ni/Si/Ni anode and enhancing the long-term stability.

Figure 5a illustrates the cycling performance of two anodes over 200 cycles. The Si thin-film anode achieved a higher initial Coulombic efficiency (ICE) of 82.6% but suffered substantial capacity fading and retained only 18.7% of its initial capacity after 200 cycles (645 mAh/g). This corresponds to a capacity decay rate of 0.41% per cycle. In contrast, the Si/Ni/Si/Ni thin-film anode (ICE = 82.2%) exhibited a lower initial capacity but exceptional cycling stability and retained 82% of its capacity after 200 cycles (1647 mAh/g) with a significantly lower decay rate of 0.09% per cycle. The superior cycling performance of the Si/Ni/Si/Ni anode can be attributed to the dual function of the Ni layer, which acts as an electrochemical barrier for preventing direct contact between Si and the electrolyte, while also providing mechanical support to mitigate Si volume changes during cycling, thereby preserving the electrode's structural integrity.

Figure 5b presents the C-rate step testing results for the Si and Si/Ni/Si/Ni thin-film anodes. The pristine silicon thin-film anode exhibited a significant capacity reduction of 67% (from 3457 mAh/g to 1120 mAh/g) as the current density increased from 0.25 mA/cm^2 to 1.5 mA/cm^2 . In comparison, the Si/Ni/Si/Ni multi-layer anode demonstrated a smaller capacity decrease of 49.6% (from 1959 mAh/g to 985 mAh/g). This result highlights the effectiveness of the nickel layers in enhancing the electrode's surface area and uniformity,

enabling faster and even lithium-ion insertion and extraction during high-rate cycling and improving the high-rate performance.

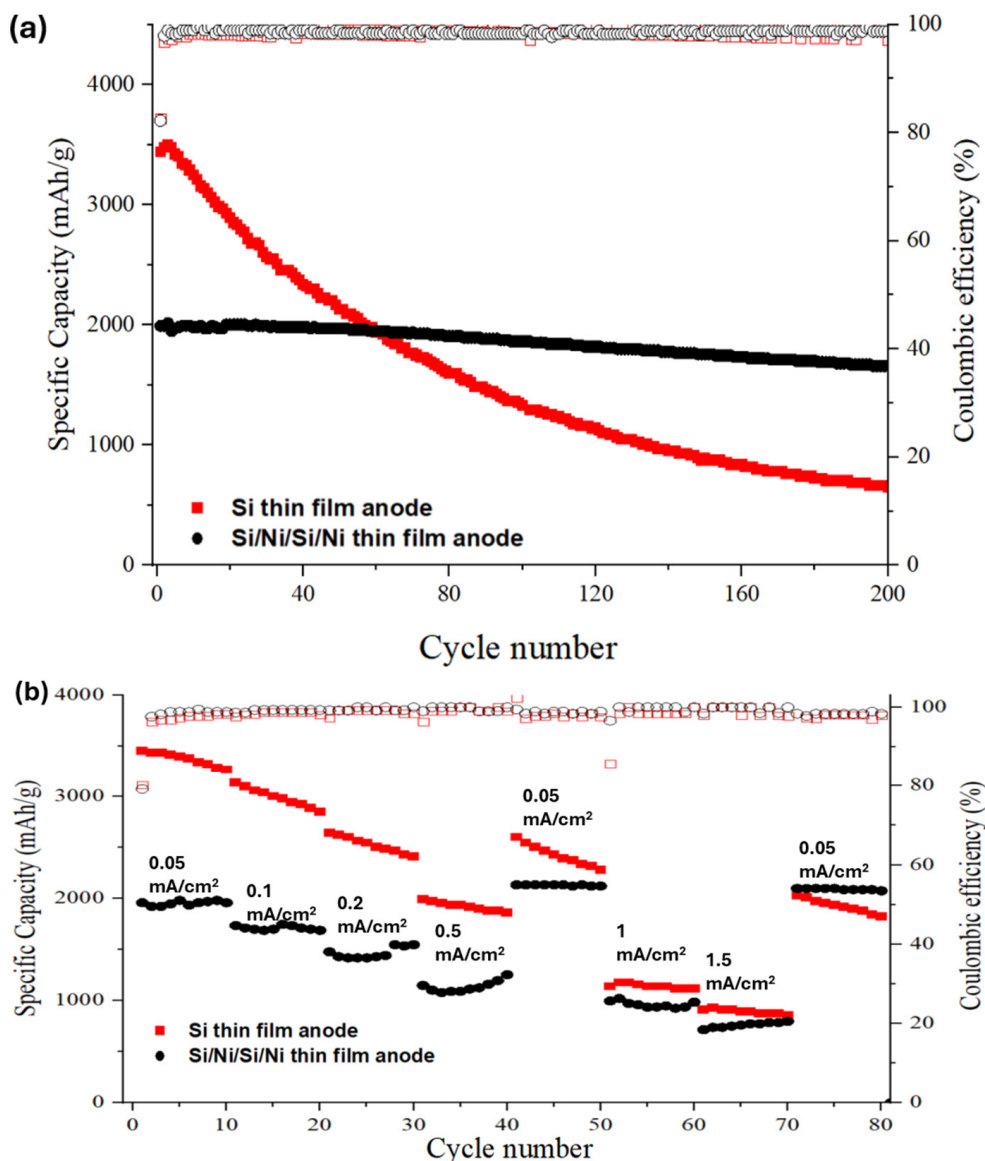


Figure 5. (a) Cycle performance of a Si thin-film anode and a Si/Ni/Si/Ni thin-film anode under test current density of $0.05 \text{ mA}/\text{cm}^2$; (b) C-rate performance of a Si thin-film anode and a Si/Ni/Si/Ni thin-film anode.

When the current density returned to $0.05 \text{ mA}/\text{cm}^2$, the Si/Ni/Si/Ni thin-film anode (2076 mAh/g) outperformed the pristine silicon thin-film anode (1823 mAh/g). This confirms that the Si/Ni/Si/Ni multi-layer structure not only suppresses the adverse effects of volume changes but also provides enhanced protection and stability for the electrode.

As depicted in Figure 6a, for the Si thin-film anode, the electrochemical reaction appears uneven, leading to the detachment of the Si film from the current collector. Further evidence is shown in Figures S2 and S3. In contrast, the Si/Ni/Si/Ni thin-film anode (Figure 6b) exhibits uniform electrochemical reactions. The Ni layer effectively improves the uniformity of Li-ion transport and maintains the physical integrity of the anode.

Figure 7a demonstrates the distinct multi-layer structure of the Si/Ni/Si/Ni thin-film anode, with a total thickness of approximately 321 nm . Figure 7b shows the cross-sectional SEM image of the Si/Ni/Si/Ni electrode after 100 cycles of discharge and charge operations

under a high current density. Although some localized uneven expansion of the silicon layer was observed, the overall structure remained intact. This indicates that the nickel layer successfully mitigated the stress induced by the volume changes of silicon during cycling.

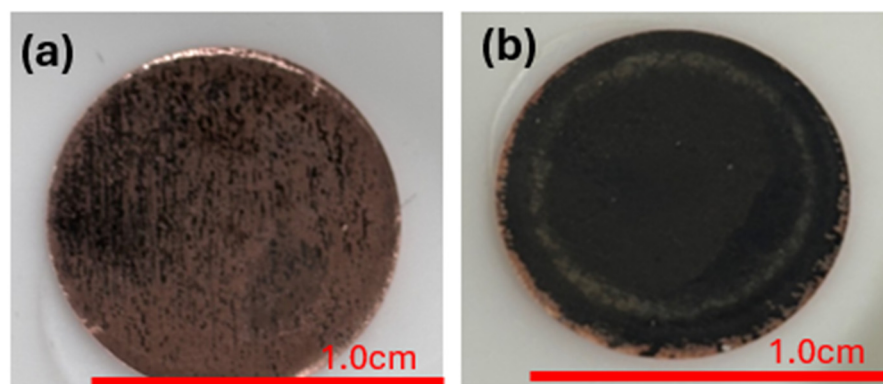


Figure 6. Optical microscope images of (a) an anode made of Si thin film and (b) an anode made of multi-layer Si/Ni/Si/Ni structure after 100 cycles of charge–discharge.

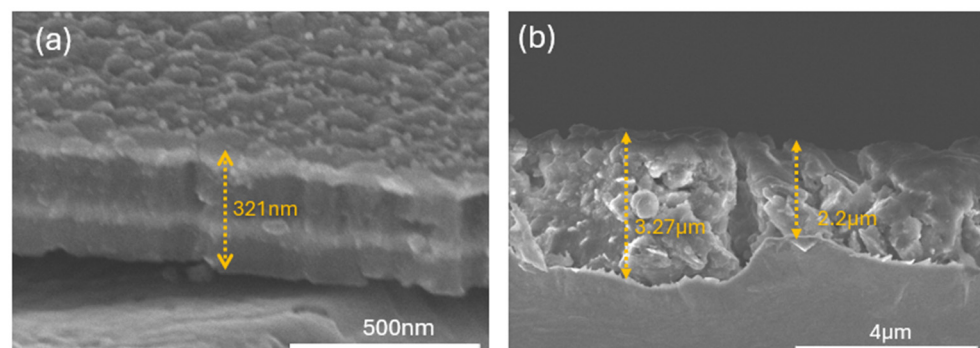


Figure 7. SEM cross-sectional images of Si/Ni/Si/Ni thin film anode (a) before and (b) after 100 cycles of discharge and charge operations under $1 \text{ mA}/\text{cm}^2$.

Figure 8a–c show that the surface of the Si thin-film anode developed significant cracks after 200 cycles. As depicted in the magnified view in Figure 8b,c, these cracks had widths of approximately $4\text{--}5 \mu\text{m}$. Their formation is attributed to the substantial volume changes of silicon during alloying and de-alloying with lithium. The volume changes generate internal stress. These cracks increase the electrode's surface area, accelerating side reactions, causing the anode to lose electrical contact with the current collector and between neighboring silicon islands. This hinders electron transport as well as lithium-ion transport, leading to a declining capacity.

Figure 8d–f shows that the surface morphology of the Si/Ni/Si/Ni thin-film anode remained relatively smooth overall, with localized cracks approximately $1 \mu\text{m}$ wide. While the Ni layer effectively mitigates large-scale crack formation, nonuniform lithium-ion transport can still cause stress concentration in certain regions, leading to small cracks. These cracks were primarily confined to specific “hotspots”, accounting for about 6% of the total surface area. Although limited in quantity, these cracks could accelerate electrolyte decomposition and gradually grow larger, with more cracks causing the long-term decline of the capacity.

X-ray photoelectron spectroscopy (XPS) analysis was used to examine the surface chemical composition. The protective role of the Ni layers and the composition of the solid electrolyte interphase (SEI) are emphasized in the analysis.

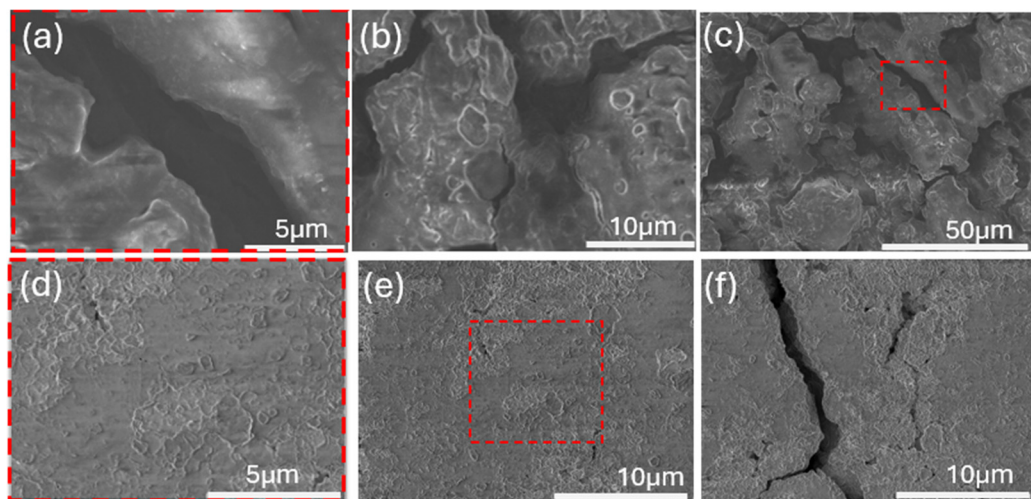


Figure 8. SEM images of a Si thin-film anode at (a–c) different magnifications after 200 cycles; SEM images of a Si/Ni/Si/Ni thin-film anode (d,e) displayed after different magnifications; (f) shows a different spot from that shown in (e) after 200 cycles.

Figure 9a,b show the C 1s XPS spectra, where the peak at 284.7 eV corresponds to C-C bonds, indicating conductive carbon, and the peak at 285.9 eV corresponds to CO_x , which is typically attributed to electrolyte decomposition. The Si/Ni/Si/Ni thin-film anode shows a notably lower peak intensity at 285.9 eV compared to the Si thin-film anode, highlighting the Ni layer's effectiveness in suppressing electrolyte decomposition and reinforcing its role as a protective barrier [30].

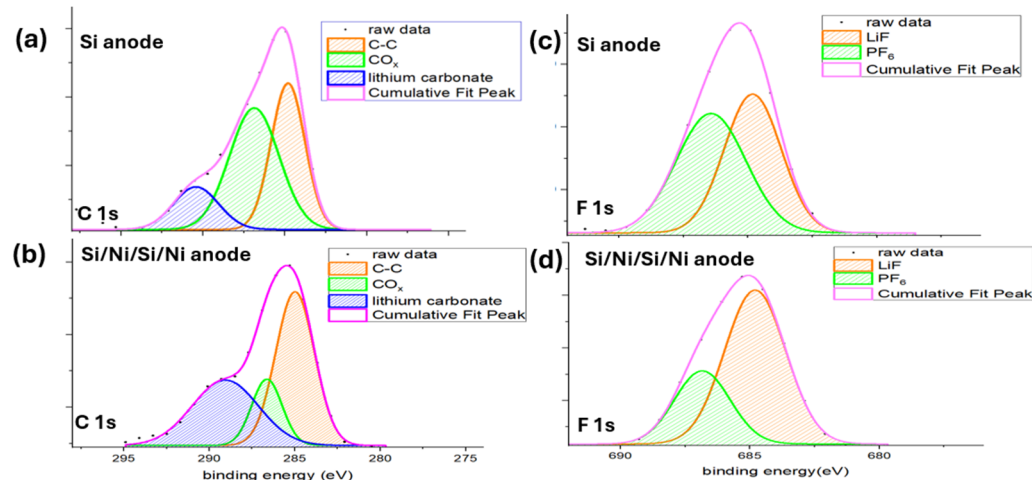


Figure 9. (a,b) C 1s and (c,d) F 1s X-ray photoelectron spectroscopy (XPS) spectra for two different electrodes after 200 cycles of charge and discharge.

Figure 9c,d show the F 1s XPS spectra, with a peak at 687 eV corresponding to PF_6^- and another at 685 eV corresponding to LiF [31,32]. The presence of LiF, a common inorganic SEI component, indicates SEI formation on the electrode surface. Known for its excellent mechanical stability, LiF suppresses electrolyte decomposition and enhances interfacial stability, thereby improving the cycling performance [33,34]. The higher LiF content observed in the Si/Ni/Si/Ni thin-film anode compared to the Si thin-film anode suggests that the Ni layer facilitates the formation of a more stable SEI, contributing to superior cycling stability.

Figure 8a illustrates significant cracks in the Si thin-film anode after cycling. The EIS analysis shown in Figure 10 indicates that these cracks contributed to an increase in both

the internal resistance (R_1) and charge transfer resistance (R_2). As Table 1 shows, the Si thin-film anode had a larger R_1 and R_2 . This is attributed to the enlarged electrode/electrolyte interfacial area caused by cracks, which accelerate the side reactions and additional growth of the SEI, and impede efficient Li-ion transport. Warburg Resistance (WR), which is the solid-state diffusion resistance for the silicon anode, was also larger than that of multi-layer Si/Ni/Si/Ni anode. This is attributed to the large surface area of the electrochemically inactive Ni layer, which results in a more stable SEI and enhances the electrode integrity.

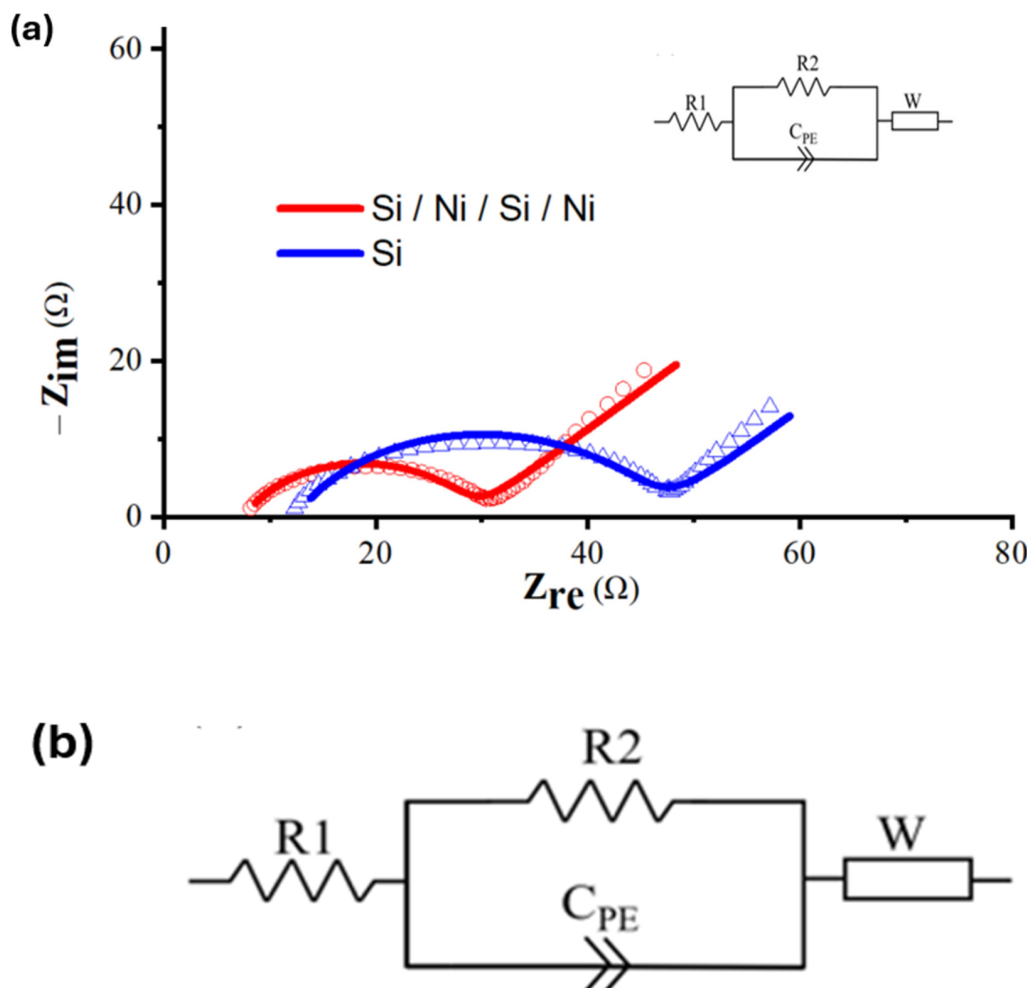


Figure 10. (a) The Nyquist plots comparing the impedance spectra of Si and Si/Ni/Si/Ni thin-film anode after 200 cycles; (b) the equivalent circuit model used to fit the impedance data.

Table 1. Comparative fitting results of EIS spectra for a Si thin-film anode and a Si/Ni/Si/Ni thin-film anode after 200 cycles of electrochemical cycling.

Sample/Resistance	$R_1(\Omega)$	$R_2(\Omega)$	$WR(\Omega)$
Si/Ni/Si/Ni thin-film anode	7.5	21.3	32.2
Si thin-film anode	13	32.9	59.7

4. Conclusions

A Si/Ni/Si/Ni multi-layer anode was studied. The Ni top layer (Figure 3b) formed relatively uniform semispherical structures and numerous pores in between and, thus, facilitated more uniform lithium-ion transport and prevented a local high lithium-ion current density and internal stress due to the irregular volume changes of the silicon. Because nickel

and its compound are more ductile than silicon, the nickel-based surface passivation layer may enhance the physical integrity of the anode. The electrochemically inert nickel layer and the compounds it forms during cycling act as a protective barrier, preventing direct contact between the electrolyte and the silicon while suppressing undesirable side reactions. Therefore, the multi-layer anode with an interlayer and a surface layer of nickel effectively accommodates silicon's substantial volume changes during charge and discharge cycling and enhances the battery's cycle life. The multi-layer anode demonstrated a significantly improved capacity retention of 82% after 200 cycles of charge–discharge. The Si/Ni/Si/Ni anode also demonstrated superior performance in C-rate tests compared to the Si anode under a high test current density.

Supplementary Materials: The following supporting information can be downloaded at: <https://www.mdpi.com/article/10.3390/batteries11020046/s1>, Table S1: Comparison of Si- and Sn-based material [35]. Table S2: Detailed peak values in CV curves; Figure S1: (a) SEM image and images of (b) Si EDS mapping and (c) Ni EDS mapping of a Si (100 nm)/Ni (20 nm)/Si (100 nm)/Ni (20 nm) anode; Figure S2: SEM cross-sectional image of Si (200 nm) anode before cycling; Figure S3: Cross-sectional EDS element content of Si (200 nm) anode after 100 cycles under 1 mA/cm^2 . Figure S4: Cyclic performance of Si (200 nm), Si (200 nm)/Ni (20 nm), Si (100 nm)/Ni (20 nm)/Si (100 nm)/Ni (20 nm), Si (66 nm)/Ni (6.6 nm)/Si (66 nm)/Ni (6.6 nm)/Si (66 nm)/Ni (6.6 nm), and Si (100 nm)/Ni (10 nm)/Si (100 nm)/Ni (10 nm) under 0.05 mA/cm^2 test current. Figure S5: Cyclic performance of Si (100 nm)/Ni (10 nm)/Si (100 nm)/Ni (10 nm) with different Si thickness under 0.05 mA/cm^2 .

Author Contributions: Y.T.: Conception, funding, data analysis, interpretation, final manuscript preparation; Y.-Y.C.: Material characterization, data analysis, device fabrication, data collection, initial data analysis, report preparation draft manuscript preparation; A.A.W.: Experimental assistance, data collection and verification, assistance to report preparation. All authors have read and agreed to the published version of the manuscript.

Funding: This research was funded by National Science and Technology Council, Taiwan under the grant number 113-2221-E-006-080-.

Data Availability Statement: The original contributions presented in this study are included in the article and Supplementary Materials. Further inquiries can be directed to the corresponding author.

Acknowledgments: The authors gratefully acknowledge the use of the scanning electron micro-scope (SEM, Hitachi-SU8000, Taipei, Taiwan) and X-ray photoelectron spectrometer (PHI Versa Probe 4, Taipei, Taiwan) belonging to the Core Facility Center of National Cheng Kung University.

Conflicts of Interest: The authors declare that they have no competing financial interests or personal relationships that appear to have influenced the work reported in this paper.

References

- Miao, Y.; Hynan, P.; Von Jouanne, A.; Yokochi, A. Current Li-ion battery technologies in electric vehicles and opportunities for advancements. *Energies* **2019**, *12*, 1074. [[CrossRef](#)]
- Gu, M.; He, Y.; Zheng, J.; Wang, C. Nanoscale silicon as anode for Li-ion batteries: The fundamentals, promises, and challenges. *Nano Energy* **2015**, *17*, 366–383. [[CrossRef](#)]
- Ko, M.; Chae, S.; Cho, J. Challenges in accommodating volume change of Si anodes for Li-ion batteries. *ChemElectroChem* **2015**, *2*, 1645–1651. [[CrossRef](#)] [[PubMed](#)]
- Hwang, T.H.; Lee, Y.M.; Kong, B.S.; Seo, J.S.; Choi, J.W. Electrospun core–shell fibers for robust silicon nanoparticle-based lithium ion battery anodes. *Nano Lett.* **2012**, *12*, 802–807. [[CrossRef](#)] [[PubMed](#)]
- Ko, M.; Chae, S.; Jeong, S.; Oh, P.; Cho, J. Elastic a-silicon nanoparticle backboned graphene hybrid as a self-compacting anode for high-rate lithium ion batteries. *ACS Nano* **2014**, *8*, 8591–8599. [[CrossRef](#)]
- Wen, Z.; Lu, G.; Mao, S.; Kim, H.; Cui, S.; Yu, K.; Huang, X.; Hurley, P.; Mao, O.; Chen, J. Silicon nanotube anode for lithium-ion batteries. *Electrochim. Commun.* **2013**, *29*, 67–70. [[CrossRef](#)]
- Park, M.H.; Kim, M.G.; Joo, J.; Kim, K.; Kim, J.; Ahn, S.; Cui, Y.; Cho, J. Silicon nanotube battery anodes. *Nano Lett.* **2009**, *9*, 3844–3847. [[CrossRef](#)]

8. Ge, M.; Rong, J.; Fang, X.; Zhou, C. Porous doped silicon nanowires for lithium ion battery anode with long cycle life. *Nano Lett.* **2012**, *12*, 2318–2323. [[CrossRef](#)]
9. Chan, C.K.; Peng, H.; Liu, G.; McIlwrath, K.; Zhang, X.F.; Huggins, R.A.; Cui, Y. High-performance lithium battery anodes using silicon nanowires. *Nat. Nanotechnol.* **2008**, *3*, 31–35. [[CrossRef](#)]
10. Abel, P.R.; Lin, Y.M.; Celio, H.; Heller, A.; Mullins, C.B. Improving the stability of nanostructured silicon thin film lithium-ion battery anodes through their controlled oxidation. *ACS Nano* **2012**, *6*, 2506–2516. [[CrossRef](#)]
11. Bates, J.B.; Dudney, N.J.; Neudecker, B.; Ueda, A.; Evans, C.D. Thin-film lithium and lithium-ion batteries. *Solid State Ionics* **2000**, *135*, 33–45. [[CrossRef](#)]
12. Zhou, M.; Cai, T.; Pu, F.; Chen, H.; Wang, Z.; Zhang, H.; Guan, S. Graphene/carbon-coated Si nanoparticle hybrids as high-performance anode materials for Li-ion batteries. *ACS Appl. Mater. Interfaces* **2013**, *5*, 3449–3455. [[CrossRef](#)] [[PubMed](#)]
13. Luo, F.; Liu, B.; Zheng, J.; Chu, G.; Zhong, K.; Li, H.; Huang, X.; Chen, L. Nano-silicon/carbon composite anode materials towards practical application for next generation Li-ion batteries. *J. Electrochem. Soc.* **2015**, *162*, A2509. [[CrossRef](#)]
14. Tzeng, Y.; Jhan, C.Y.; Sung, S.H.; Chiou, Y.Y. Effects of Crystalline Diamond Nanoparticles on Silicon Thin Films as an Anode for a Lithium-Ion Battery. *Batteries* **2024**, *10*, 321. [[CrossRef](#)]
15. Sethuraman, V.A.; Kowollik, K.; Srinivasan, V. Increased cycling efficiency and rate capability of copper-coated silicon anodes in lithium-ion batteries. *J. Power Sources* **2011**, *196*, 393–398. [[CrossRef](#)]
16. Luo, W.; Chen, X.; Xia, Y.; Chen, M.; Wang, L.; Wang, Q.; Li, W.; Yang, J. Surface and interface engineering of silicon-based anode materials for lithium-ion batteries. *Adv. Energy Mater.* **2017**, *7*, 1701083. [[CrossRef](#)]
17. Chen, Z.; Soltani, A.; Chen, Y.; Zhang, Q.; Davoodi, A.; Hosseinpour, S.; Peukert, W.; Liu, W. Emerging organic surface chemistry for Si anodes in lithium-ion batteries: Advances, prospects, and beyond. *Adv. Energy Mater.* **2022**, *12*, 2200924. [[CrossRef](#)]
18. Li, H.; Bai, H.; Tao, Z.; Chen, J. Si–Y multi-layer thin films as anode materials of high-capacity lithium-ion batteries. *J. Power Sources* **2012**, *217*, 102–107. [[CrossRef](#)]
19. Kim, J.B.; Lee, H.Y.; Lee, K.S.; Lim, S.H.; Lee, S.M. Fe/Si multi-layer thin film anodes for lithium rechargeable thin film batteries. *Electrochim. Commun.* **2003**, *5*, 544–548. [[CrossRef](#)]
20. Tong, L.; Wang, P.; Chen, A.; Qiu, F.; Fang, W.; Yang, J.; Wang, C.; Yang, Y. Improved electrochemical performance of binder-free multi-layered silicon/carbon thin film electrode for lithium-ion batteries. *Carbon* **2019**, *153*, 592–601. [[CrossRef](#)]
21. Salah, M.; Hall, C.; Yap, P.L.; Fabretto, M. Silicon-tin thin-film anodes for low and high power-density lithium-ion batteries. *Thin Solid Films* **2024**, *796*, 140332. [[CrossRef](#)]
22. Fu, H.; Gu, F.; Niu, Y.; Liao, S.; Bu, Z.; Wang, H.; Yang, D.; Wang, X.; Li, Q. Spatially confined transition metals boost high initial coulombic efficiency in alloy anodes. *Chem. Sci.* **2024**, *16*, 418–424. [[CrossRef](#)] [[PubMed](#)]
23. Wang, K.-X.; Li, X.-H.; Chen, J.-S. Surface and interface engineering of electrode materials for lithium-ion batteries. *Adv. Mater.* **2015**, *27*, 527–545. [[CrossRef](#)] [[PubMed](#)]
24. Song, R.; Song, H.; Zhou, J.; Chen, X.; Wu, B.; Yang, H.Y. Hierarchical porous carbon nanosheets and their favorable high-rate performance in lithium-ion batteries. *J. Mater. Chem.* **2012**, *22*, 12369–12374. [[CrossRef](#)]
25. Deng, L.; Cui, Y.; Chen, J.; Wu, J.; Baker, A.P.; Li, Z.; Zhang, X. A core-shell Si@NiSi₂/Ni/C nanocomposite as an anode material for lithium-ion batteries. *Electrochim. Acta* **2016**, *192*, 303–309. [[CrossRef](#)]
26. Zhang, W.; Cai, T.H.; Sheldon, B.W. The impact of initial SEI formation conditions on strain-induced capacity losses in silicon electrodes. *Adv. Energy Mater.* **2019**, *9*, 1803066. [[CrossRef](#)]
27. Joshi, T.; Eom, K.; Yushin, G.; Fuller, T.F. Effects of dissolved transition metals on the electrochemical performance and SEI growth in lithium-ion batteries. *J. Electrochem. Soc.* **2014**, *161*, A1915. [[CrossRef](#)]
28. Tokranov, A.; Kumar, R.; Li, C.; Minne, S.; Xiao, X.; Sheldon, B.W. Control and optimization of the electrochemical and mechanical properties of the solid electrolyte interphase on silicon electrodes in lithium ion batteries. *Adv. Energy Mater.* **2016**, *6*, 1502302. [[CrossRef](#)]
29. Huang, X.; Pu, H.; Chang, J.; Cui, S.; Hallac, P.B.; Jiang, J.; Hurley, P.; Chen, J. Improved cyclic performance of Si anodes for lithium-ion batteries by forming intermetallic interphases between Si nanoparticles and metal microparticles. *ACS Appl. Mater. Interfaces* **2013**, *5*, 11965–11970. [[CrossRef](#)]
30. Jaumann, T.; Balach, J.; Klose, M.; Oswald, S.; Langklotz, U.; Michaelis, A.; Eckert, J.; Giebel, L. SEI-component formation on sub 5 nm sized silicon nanoparticles in Li-ion batteries: The role of electrode preparation, FEC addition and binders. *Phys. Chem. Chem. Phys.* **2015**, *17*, 24956–24967. [[CrossRef](#)]
31. Etacheri, V.; Haik, O.; Goffer, Y.; Roberts, G.A.; Stefan, I.C.; Fasching, R.; Aurbach, D. Effect of fluoroethylene carbonate (FEC) on the performance and surface chemistry of Si-nanowire Li-ion battery anodes. *Langmuir* **2012**, *28*, 965–976. [[CrossRef](#)] [[PubMed](#)]
32. Philippe, B.; Dedryvère, R.; Allouche, J.; Lindgren, F.; Gorgoi, M.; Rensmo, H.; Gonbeau, D.; Edström, K. Nanosilicon electrodes for lithium-ion batteries: Interfacial mechanisms studied by hard and soft X-ray photoelectron spectroscopy. *Chem. Mater.* **2012**, *24*, 1107–1115. [[CrossRef](#)]

33. Tan, J.; Matz, J.; Dong, P.; Shen, J.; Ye, M. A growing appreciation for the role of LiF in the solid electrolyte interphase. *Adv. Energy Mater.* **2021**, *11*, 2100046. [[CrossRef](#)]
34. Kim, K.H.; Cho, J.H.; Hwang, J.U.; Im, J.S.; Lee, Y.S. A key strategy to form a LiF-based SEI layer for a lithium-ion battery anode with enhanced cycling stability by introducing a semi-ionic CF bond. *J. Ind. Eng. Chem.* **2021**, *99*, 48–54. [[CrossRef](#)]
35. Li, W.; Sun, X.; Yu, Y. Si-, Ge-, Sn-based anode materials for lithium-ion batteries: From structure design to electrochemical performance. *Small Methods.* **2017**, *1*, 1600037. [[CrossRef](#)]

Disclaimer/Publisher’s Note: The statements, opinions and data contained in all publications are solely those of the individual author(s) and contributor(s) and not of MDPI and/or the editor(s). MDPI and/or the editor(s) disclaim responsibility for any injury to people or property resulting from any ideas, methods, instructions or products referred to in the content.